PERGAMON

International Journal of Solids and Structures 37 (2000) 3055–3078

INTERNATIONAL JOURNAL OF SOLIDS and STRUCTURES

www.elsevier.com/locate/ijsolstr

Torsional buckling analysis of thin and thick shells of revolution

Dongyao Tan

Department of Aeronautics, Imperial College of Science, Technology and Medicine, Prince Consort Road, London SW7 2BY, UK

Received 5 March 1998; in revised form 8 April 1999

Abstract

Based on the classical thin shell theory and the first-order shear deformation shell theory, two models are developed in this paper for predicting the torsional buckling loads of thin and thick shells of revolution. The material property of a shell of revolution is described as a general type of laminated composites and natural coordinates are used to define its geometry in which any kind of kinematic boundary condition can be applied precisely. To effectively use the axi-symmetric property of a shell of revolution in the analysis, a multi-level substructuring technique is employed in which only one substructure is involved in each substructuring level so the size of the problem in real computation is always kept very small. The torsional buckling behaviours of a circular cylinder, a conic shell, an elliptic hyperboloid shell and an ellipsoid shell are investigated using these models.

Keywords: Torsional buckling; Shells of revolution; Laminated composites; Substructure

1. Introduction

Buckling behaviours of doubly curved shells are often related to their large deflection processes and the geometric nonlinearity must be considered, which usually brings great difficulty for their analytical and numerical analysis. Extensive study has been given to this problem for several decades (for detail surveys, see e.g. Stolarski et al., 1995; Crisfield et al., 1992). Various numerical simulations have been generated to show the detailed buckling and post-buckling processes (such as the full equilibrium path in the typical snap-through phenomenon). Besides the nonlinearity related buckling behaviours of the doubly curved shells, there still is a particular buckling problem for a special type of doubly curved shell — shells of revolution — which can be accommodated in the linear shell theory. Torsional buckling of shells of revolution is such a problem. Unfortunately, it has not been given much investigation before either analytically or numerically.

Fig. 1 shows a shell of revolution subjected to torques acting at its two ends. The pre-buckling shear

0020-7683/00/$ - see front matter
PII: S0020-7683(99)00120-1

stress in the shell of revolution can be determined using the static equilibrium condition as follows,

$$\tau(s) = \frac{T}{2\pi h y^2(s)}. \tag{1}$$

The pre-buckling deformation of the shell of revolution under the action of torques is assumed small and within its original surface. Therefore, linear shell theory can be applied. When the shell of revolution undergoes torsional buckling, the displacements out of the original surface develop.

This paper proposes a numerical method in the context of both the first-order shear deformation shell theory (SDST) and the classical thin shell theory (TST) to analyze the torsional buckling behaviour of a shell of revolution with thick or thin geometry. The shell of revolution is circumferentially discretized by the meridians and, in each element, the general spline functions are used to represent the displacement variations along the meridians and Lagrangian and Hermitian polynomials are used to represent the displacement variations in the circumferential direction. So the shape function of an element is a mix of the spline function family and the Lagrangian and Hermitian polynomial family. In the proposed method and its software implementation, there is no limit for the degree of spline functions used in the interpolation for displacements. So, by choosing a higher degree for spline functions, a higher order of displacement continuity along the meridians can be preserved if required. Without introducing much difficulty and complexity, the method models the material property of a shell of revolution as a general type of laminated composites for the purpose to accommodate a wide variety shells of revolution used in different engineering branches like aerospace engineering, maritime engineering and civil engineering. In geometric description, this method chooses natural coordinates as a base so that any kind of kinematic boundary condition along the meridians and on the crosswise end-edges of a shell of revolution can be prescribed precisely. In finding the torsional buckling loads for a shell of revolution, the Sturm sequence method (Wittrick and Williams, 1971; Gupta, 1972) is used incorporated with a multi-level substructuring technique. The torsional buckling behaviours of a circular cylinder, a conic shell, an elliptic hyperboloid shell and an ellipsoid shell are investigated with respect to the different kinds of material property that they have.

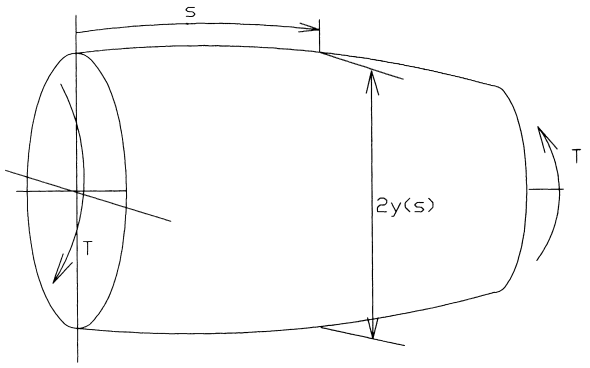

Fig. 1. A shell of revolution.

2. Displacement representation of an element

2.1. Geometry description of an element

Fig. 2 shows a basic element of a shell of revolution which may, in general, be a laminate having arbitrary lay-up of a number of layers of fibre-reinforced composite material. In the element, the natural coordinates are used. For a shell of revolution, this natural coordinate system is orthogonal and happens to be the lines of curvature.

According to the first-order shear deformation shell theory (see, e.g. Reddy, 1984; Leissa and Chang, 1996), the behaviour of the shell is characterized by the five fundamental displacement-type quantities indicated in Fig. 2, namely u, v and w, the translational displacements at the middle surface in the s, t and z directions, respectively, and ψ_s and ψ_t, the rotations of the middle-surface normal along the s and t directions, respectively. However, in the classical thin shell theory, the Kirchhoff normalcy condition is invoked and the rotations ψ_s and ψ_t are directly related to the deflection w and the displacements u and v by the way of equations:

$$\psi_s = \frac{u}{R_s} - \frac{\partial w}{\partial s}, \psi_t = \frac{v}{R_t} - \frac{\partial w}{\partial t}. \tag{2}$$

It follows, of course, that shell behaviour in TST analysis can be represented by three fundamental quantities, namely u, v and w, rather than the five fundamental quantities of SDST analysis.

In the present approach, the physical displacements are only specified at some locations on several so called reference meridians. The displacements elsewhere in an element are interpolated from them. On the reference meridians, the spline interpolation is used which facilitates the required displacement continuity along the meridians to be maintained and the kinematic boundary condition at two ends of the shells to be satisfied. Between the reference meridians, the polynomial interpolation is used which observes the condition that no additional physical displacements are needed other than those specified on the reference meridians.

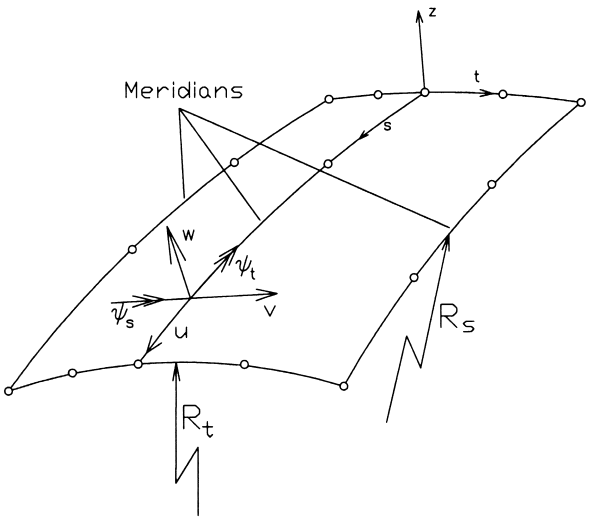

Fig. 2. An element.

2.2. Displacement representation along a meridian

Let $b_{m,n}(s)$ be a basis spline function of degree m defined on a reference meridian with a knot sequence $\{s_n\}$. It can be proved that the basis spline function is unique and can be expressed as a linear combination of so-called truncated power functions (see, e.g. Schempp, 1982), i.e.

$$b_{m,n}(s) = \sum_{0 \le k \le m+1} a_{k,n}(s - s_{n+k})_+^m, \tag{3}$$

where $(s-s_{n+k})_+ = \sup(s-s_{n+k}, 0)$. To satisfy the continuity, finite support and normal conditions of a basis spline function, the real coefficients $a_{k,n}$ ($k = 0, 1, 2,..., m+1$) are determined by the following equations:

$$\sum_{0 \le k \le m+1} a_{k,n}(s_l - s_{n+k})^m = 0, \ (l = n+1, \ldots, n+m+1) \tag{4}$$

$$\sum_{0 \le k \le m+1} a_{k,n}(s_{n+m+1} - s_{n+k})^{m+1} = m+1. \tag{5}$$

Let $f(s, t)$ be a continuous displacement function, for example it may be $u(s, t)$, $v(s, t)$, $w(s, t)$, $\psi_s(s, t)$ or $\psi_t(s, t)$. When t is constrained on the ith reference meridian, i.e. $t = t_i(s)$, $f(s, t_i(s))$ becomes a continuous function on it. So, $f(s, t_i(s))$ can be approximated by the spline interpolation as follows,

$$f(s,t_i(s)) = \sum_{n=1}^{N_s} \alpha_n b_{m,n}(s), \tag{6}$$

where α_n ($n = 1, 2,..., N_s$) are interpolation coefficients which should be determined by the specified conditions of $f(s, t_i(s))$ on the reference meridian, and N_s is the total number of basis splines used for the meridian. The specified conditions of $f(s, t_i(s))$ are chosen to be:

$$\begin{aligned} \mathbf{f}_i = \big[& f(s_1, t_i(s_1)), f^{(1)}(s_1, t_i(s_1)), \ldots, f^{(m_l)}(s_1, t_i(s_1)), f(s_2, t_i(s_2)), f(s_3, t_i(s_3)), \ldots, \\ & f(s_{N_s-m}, t_i(s_{N_s-m})), f^{(1)}(s_{N_s-m}, t_i(s_{N_s-m})), \ldots, f^{(m_r)}(s_{N_s-m}, t_i(s_{N_s-m})) \big]^T, \end{aligned} \tag{7}$$

where $m_l = m/2 - \mathrm{mod}(m,2)$, $m_r = m - m_l - 1$ and $f^{(k)}(s_l, t_i(s_l))$ ($k = 0, 1, 2,..., m_l$) and $f^{(k)}(s_{N_s-m}, t_i(s_{N_s-m}))$ ($k = 0, 1, 2,..., m_r$) are values of the displacement function and its derivatives at two ends of a shell element where the kinematic boundary conditions may be enforced.

Substituting these specified conditions in Eq. (6), the obtained $\alpha = [\alpha_1, \alpha_2,..., \alpha_n]^T$ are,

$$\alpha = \mathbf{R}^{-1}\mathbf{f}_i, \tag{8}$$

where the elements of $\mathbf{R}$ are,

$$\mathbf{R}_{l,k} = \begin{cases} b_{m,k}^{(n)}(s_l), & (l = n+1;\ n = 0,1,\ldots,m_l;\ k = 1,2,\ldots,N_s); \\ b_{m,k}(s_n), & (l = n+m_l;\ n = 2,3,\ldots,N_s-m;\ k = 1,2,\ldots,N_s); \\ b_{m,k}^{(n)}(s_{N_s-m+1}), & (l = n+N_s-m_r;\ n = 0,1,\ldots,m_r;\ k = 1,2,\ldots,N_s). \end{cases} \tag{9}$$

Combining Eqs. (6) and (8), the spline interpolation of $f(s, t_i(s))$ with its specified values is,

$$f(s,t_i(s)) = \mathbf{B}_m(s)\mathbf{f}_i, \tag{10}$$

where

$$\mathbf{B}_m(s) = [b_{m,1}(s), b_{m,2}(s), \ldots, b_{m,N_s}(s)]\mathbf{R}^{-1}. \tag{11}$$

2.3. Displacement representation in the circumferential direction in SDST

When s is fixed, $f(s, t)$ becomes a continuous function in the circumferential t-direction whose values are restricted to $f(s, t_i(s))$ on its junctions with the reference meridians. As only C^0-type continuity is required on the displacements in SDST, the Lagrangian polynomial interpolation could be used in this direction. Therefore, $f(s, t)$ can be approximated as,

$$f(s,t) = \sum_{i=1}^{i_p} P_i(t, s) f(s, t_i(s)), \tag{12}$$

where $P_i(t, s)$ ($i = 1, 2,..., i_p$) are Lagrangian polynomial functions, for instance when $i_p = 4$, they are,

$$P_1(\eta) = \frac{(-1 + \eta + 9\eta^2 - 9\eta^3)}{16},$$

$$P_2(\eta) = \frac{(9 - 27\eta - 9\eta^2 + 27\eta^3)}{16},$$

$$P_3(\eta) = \frac{(9 + 27\eta - 9\eta^2 - 27\eta^3)}{16}$$

$$P_4(\eta) = \frac{(-1 - \eta + 9\eta^2 + 9\eta^3)}{16}, \tag{13}$$

where $\eta = 2t/l_t(s)$, and $l_t(s)$ is the circumferential arc length of the element at the position s on the meridian.

2.4. Displacement representation in the circumferential direction in TST

In classical thin shell theory, the continuity requirement on displacements $u(s, t)$ and $v(s, t)$ is the same as that in SDST. So, they can be approximated in the same way as before using Eq. (12). However, as the Kirchhoff normalcy condition expressed by Eq. (2) the requirement of the C^1-type continuity of $w(s, t)$ is necessary. That means the first derivatives of $w(s, t)$ in the circumferential direction (i.e. $\partial w(s,t)/\partial t$) should be used as freedoms at the outside meridians of the element. This condition limits the choice of the interpolation functions for $w(s,t)$ in the circumferential direction. When $i_p = 4$, Hermitian functions satisfy this condition. They are,

$$P_{1H}(\eta) = \frac{(2 - 3\eta + \eta^3)}{4},$$

$$P_{2\mathrm{H}}(\eta) = \frac{b(1-\eta-\eta^2+\eta^3)}{8},$$

$$P_{3\mathrm{H}}(\eta) = \frac{b(-1-\eta+\eta^2+\eta^3)}{8}$$

$$P_{4\mathrm{H}}(\eta) = \frac{(2+3\eta-\eta^3)}{4}, \tag{14}$$

where $\eta = 2t/l_t(s)$. It should be noted that $P_{1\mathrm{H}}(\eta)$ and $P_{2\mathrm{H}}(\eta)$ are both associated with reference meridian 1 and related to degrees of freedom corresponding to $w(s, t)$ and $\partial w(s, t)/\partial t$, respectively, so do $P_{4\mathrm{H}}(\eta)$ and $P_{3\mathrm{H}}(\eta)$ with reference meridian 4 (Here, reference meridians 1 and 4 are the two outside reference meridians of the shell element).

In summary, the displacement field of an element in SDST can be constructed as,

$$u(s,t) = \sum_{i=1}^{i_p} P_i(t, s)\mathbf{B}_{m_u}(s)\mathbf{u}_i, \tag{15}$$

$$v(s,t) = \sum_{i=1}^{i_p} P_i(t, s)\mathbf{B}_{m_v}(s)\mathbf{v}_i, \tag{16}$$

$$w(s,t) = \sum_{i=1}^{i_p} P_i(t, s)\mathbf{B}_{m_w}(s)\mathbf{w}_i, \tag{17}$$

$$\psi_t(s, t) = \sum_{i=1}^{i_p} P_i(t, s)\mathbf{B}_{m_{\psi_t}}(s)\psi_{ti} \tag{18}$$

$$\psi_s(s,t) = \sum_{i=1}^{i_p} P_i(t, s)\mathbf{B}_{m_{\psi_s}}(s)\psi_{si}. \tag{19}$$

where m_u, m_v, m_w, m_{ψ_t} and m_{ψ_s} are the degrees of the basis spline functions used for interpolating u, v, w, ψ_t and ψ_s, respectively. And the displacement field of an element in TST are expressed by Eqs. (15) and (16) and the following equation,

$$w(s,t) = \sum_{i=1}^{4} P_{i\mathrm{H}}(t, s)\mathbf{B}_{m_w}(s)\mathbf{w}_i. \tag{20}$$

As noted before, $\mathbf{w}_2$ and $\mathbf{w}_3$ in the above equation are not the displacements associated with reference meridians 2 and 3. They are actually $\partial\mathbf{w}_1/\partial t$ and $\partial\mathbf{w}_4/\partial t$, respectively.

3. Characteristic matrices of a SDST element

3.1. Constitutive equations

Within the context of first-order SDST the linear constitutive equations for an arbitrary laminate are,

$$\mathbf{F} = \mathbf{L}\mathbf{e}, \tag{21}$$

where

$$\mathbf{F} = [N_s, N_t, N_{st}, M_s, M_t, M_{st}, Q_t, Q_s]^T, \tag{22}$$

$$\mathbf{L} = \begin{bmatrix} A_{11} & A_{12} & A_{16} & B_{11} & B_{12} & B_{16} & 0 & 0 \\ & A_{22} & A_{26} & B_{21} & B_{22} & B_{26} & 0 & 0 \\ & & A_{66} & B_{61} & B_{62} & B_{66} & 0 & 0 \\ & & & D_{11} & D_{12} & D_{16} & 0 & 0 \\ & \text{Sym.} & & & D_{22} & D_{26} & 0 & 0 \\ & & & & & D_{66} & 0 & 0 \\ & & & & & & A_{44} & A_{45} \\ & & & & & & & A_{55} \end{bmatrix} \tag{23}$$

$$\mathbf{e} = \begin{bmatrix} \dfrac{\partial u}{\partial s} + \dfrac{w}{R_s} \\ \dfrac{\partial v}{\partial t} + \dfrac{w}{R_t} \\ \dfrac{\partial u}{\partial t} + \dfrac{\partial v}{\partial s} \\ \dfrac{\partial \psi_s}{\partial s} \\ \dfrac{\partial \psi_t}{\partial t} \\ \dfrac{\partial \psi_s}{\partial t} + \dfrac{\partial \psi_t}{\partial s} + \dfrac{1}{2}\left(\dfrac{1}{R_t} - \dfrac{1}{R_s}\right)\left(\dfrac{\partial v}{\partial s} - \dfrac{\partial u}{\partial t}\right) \\ \dfrac{\partial w}{\partial t} + \psi_t - \dfrac{v}{R_t} \\ \dfrac{\partial w}{\partial s} + \psi_s - \dfrac{u}{R_s} \end{bmatrix}. \tag{24}$$

The laminate stiffness coefficients in Eq. (23) are defined in the standard way (see, e.g. Reddy, 1984; Leissa and Chang, 1996). The explicit expression of the strain vector **e** in the specified values of the displacement field can be obtained as follows using Eqs. (15)–(19).

$$\mathbf{e} = \sum_{i=1}^{i_p} \mathbf{\Phi}_i \mathbf{d}_i, \tag{25}$$

where $\mathbf{d}_i = [\mathbf{u}_i^T, \mathbf{v}_i^T, \mathbf{w}_i^T, \boldsymbol{\psi}_{ti}^T, \boldsymbol{\psi}_{si}^T]^T$ and

$$\mathbf{\Phi}_i = \begin{bmatrix} P_i\mathbf{B}'_{m_u} & 0 & \frac{1}{R_s}P_i\mathbf{B}_{m_w} & 0 & 0 \\ 0 & P'_i\mathbf{B}_{m_v} & \frac{1}{R_s}P_i\mathbf{B}_{m_w} & 0 & 0 \\ P'_i\mathbf{B}_{m_u} & P_i\mathbf{B}'_{m_v} & 0 & 0 & 0 \\ 0 & 0 & 0 & 0 & P_i\mathbf{B}'_{m_{\psi_s}} \\ 0 & 0 & 0 & P'_i\mathbf{B}_{m_{\psi_t}} & 0 \\ \frac{1}{2}\left(\frac{1}{R_s}-\frac{1}{R_t}\right)P'_i\mathbf{B}_{m_u} & \frac{1}{2}\left(\frac{1}{R_t}-\frac{1}{R_s}\right)P_i\mathbf{B}'_{m_v} & 0 & P_i\mathbf{B}'_{m_{\psi_t}} & P'_i\mathbf{B}_{m_{\psi_s}} \\ 0 & -\frac{1}{R_t}P_i\mathbf{B}_{m_v} & P'_i\mathbf{B}_{m_w} & P_i\mathbf{B}_{m_{\psi_t}} & 0 \\ -\frac{1}{R_s}P_i\mathbf{B}_{m_u} & 0 & P_i\mathbf{B}'_{m_w} & 0 & P_i\mathbf{B}_{m_{\psi_s}} \end{bmatrix} \tag{26}$$

in which ‘′’ represents the derivative of a function or function vector with respect to its variable.

3.2. Stiffness matrix

The strain energy of an element is,

$$U = \frac{1}{2}\int_0^{l_s}\int_{-l_t(s)/2}^{l_t(s)/2}\mathbf{e}^T\mathbf{L}\mathbf{e}\,\mathrm{d}t\,\mathrm{d}s. \tag{27}$$

Its quadratic form in the specified values of the displacement field is what follows after substituting Eq. (25) into Eq. (27),

$$U = \frac{1}{2}\int_0^{l_s}\int_{-l_t(s)/2}^{l_t(s)/2}\sum_{i=1}^{i_p}\sum_{j=1}^{i_p}\mathbf{d}_i^T\mathbf{\Phi}_i^T\mathbf{L}\mathbf{\Phi}_j\mathbf{d}_j\,\mathrm{d}t\,\mathrm{d}s = \frac{1}{2}\mathbf{d}^T\mathbf{k}\mathbf{d}, \tag{28}$$

where $\mathbf{d}=[\mathbf{d}_1^T, \mathbf{d}_2^T, \ldots, \mathbf{d}_{i_p}^T]^T$ and,

$$\mathbf{k} = \left[\int_0^{l_s}\int_{-l_t(s)/2}^{l_t(s)/2}\mathbf{\Phi}_i^T\mathbf{L}\mathbf{\Phi}_j\,\mathrm{d}t\,\mathrm{d}s\right]. \tag{29}$$

Matrix $\mathbf{k}$ is the stiffness matrix of the element.

3.3. Geometric stiffness matrix

The potential energy of the applied shear stress is,

$$V = \frac{1}{2}T\int_0^{l_s}\int_{-l_t(s)/2}^{l_t(s)/2}\mathbf{e}_{NL}^T\mathbf{S}\mathbf{e}_{NL}\,\mathrm{d}t\,\mathrm{d}s, \tag{30}$$

where T is the torque and

$$\mathbf{e}_{NL} = \left[\frac{\partial u}{\partial s} + \frac{w}{R_s}, \frac{\partial u}{\partial t}, \frac{\partial v}{\partial s}, \frac{\partial v}{\partial t} + \frac{w}{R_t}, \frac{\partial w}{\partial s} - \frac{u}{R_s}, \frac{\partial w}{\partial t} - \frac{v}{R_t}, \frac{\partial \psi_t}{\partial s}, \frac{\partial \psi_t}{\partial t}, \frac{\partial \psi_s}{\partial s}, \frac{\partial \psi_s}{\partial t}\right]^T, \tag{31}$$

$$\mathbf{S} = \frac{1}{2\pi y^2(s)}\begin{bmatrix} 0 & 1 & & & & & & & & \\ 1 & 0 & & & & & & & & \\ & & 0 & 1 & & & & & & \\ & & 1 & 0 & & & & & & \\ & & & & 0 & 1 & & & & \\ & & & & 1 & 0 & & & & \\ & & & & & & 0 & \frac{h^2}{12} & & \\ & & & & & & \frac{h^2}{12} & 0 & & \\ & & & & & & & & 0 & \frac{h^2}{12} \\ & & & & & & & & \frac{h^2}{12} & 0 \end{bmatrix}. \tag{32}$$

The explicit expression of $\mathbf{e}_{NL}$ in the specified values of the displacement field can be obtained as follows using Eqs. (15)–(19),

$$\mathbf{e}_{NL} = \sum_{i=1}^{i_p} \mathbf{\Psi}_i \mathbf{d}_i, \tag{33}$$

where

$$\Psi_i = \begin{bmatrix} P_i\mathbf{B}'_{m_u} & 0 & \frac{1}{R_s}P_i\mathbf{B}_{m_w} & 0 & 0 \\ P'_i\mathbf{B}_{m_u} & 0 & 0 & 0 & 0 \\ 0 & P_i\mathbf{B}'_{m_v} & 0 & 0 & 0 \\ 0 & P'_i\mathbf{B}_{m_v} & \frac{1}{R_t}P_i\mathbf{B}_{m_w} & 0 & 0 \\ -\frac{1}{R_s}P_i\mathbf{B}_{m_u} & 0 & P_i\mathbf{B}'_{m_w} & 0 & 0 \\ 0 & -\frac{1}{R_t}P_i\mathbf{B}_{m_v} & P'_i\mathbf{B}_{m_w} & 0 & 0 \\ 0 & 0 & 0 & P_i\mathbf{B}'_{m_{\psi_t}} & 0 \\ 0 & 0 & 0 & 0 & P_i\mathbf{B}'_{m_{\psi_s}} \\ 0 & 0 & 0 & 0 & P'_i\mathbf{B}_{m_{\psi_s}} \end{bmatrix}. \tag{34}$$

Similarly, the quadratic form of the potential energy in the specified values of the displacement field can be obtained as follows using Eq. (30),

$$V = \frac{1}{2}T\int_0^{l_s}\int_{-l_t(s)/2}^{l_t(s)/2}\sum_{i=1}^{i_p}\sum_{j=1}^{i_p}\mathbf{d}_i^T\boldsymbol{\Psi}_i^T\mathbf{S}\boldsymbol{\Psi}_j\mathbf{d}_j\,\mathrm{d}t\,\mathrm{d}s = \frac{1}{2}\mathbf{d}^T(T\mathbf{k}_g)\mathbf{d}, \tag{35}$$

where

$$\mathbf{k}_g = \left[\int_0^{l_s}\int_{-l_t(s)/2}^{l_t(s)/2}\boldsymbol{\Psi}_i^T\mathbf{S}\boldsymbol{\Psi}_j\,\mathrm{d}t\,\mathrm{d}s\right]. \tag{36}$$

Matrix $T\mathbf{k}_g$ is the geometric stiffness matrix of the element of the shell of revolution subjected to torque T.

4. Characteristic matrices of a TST element

4.1. Constitutive equations

These can again be expressed by the matrix equation Eq. (21). But the definitions of **F**, **L** and **e** change to,

$$\mathbf{F} = [N_s,\, N_t,\, N_{st},\, M_s,\, M_t,\, M_{st}]^T, \tag{37}$$

$$\mathbf{L} = \begin{bmatrix} A_{11} & A_{12} & A_{16} & B_{11} & B_{12} & B_{16} \\ & A_{22} & A_{26} & B_{21} & B_{22} & B_{26} \\ & & A_{66} & B_{61} & B_{62} & B_{66} \\ & & & D_{11} & D_{12} & D_{16} \\ & \text{Sym.} & & & D_{22} & D_{16} \\ & & & & & D_{66} \end{bmatrix}, \tag{38}$$

$$\mathbf{e} = \begin{bmatrix} \dfrac{\partial u}{\partial s} + \dfrac{w}{R_s} \\ \dfrac{\partial v}{\partial t} + \dfrac{w}{R_t} \\ \dfrac{\partial u}{\partial t} + \dfrac{\partial v}{\partial s} \\ -\dfrac{\partial^2 w}{\partial s^2} + \dfrac{1}{R_s}\dfrac{\partial u}{\partial s} \\ -\dfrac{\partial^2 w}{\partial t^2} + \dfrac{1}{R_t}\dfrac{\partial v}{\partial t} \\ -2\dfrac{\partial^2 w}{\partial s\partial t} + \dfrac{1}{2}\left(\dfrac{3}{R_t} - \dfrac{1}{R_s}\right)\dfrac{\partial v}{\partial s} + \dfrac{1}{2}\left(\dfrac{3}{R_s} - \dfrac{1}{R_t}\right)\dfrac{\partial u}{\partial t} \end{bmatrix}. \tag{39}$$

In obtaining Eq. (39) from Eq. (24), the Kirchhoff normalcy condition (2) has been used.

Substituting Eqs. (15), (16) and (20) into Eq. (39) obtains the explicit expression of **e** in the specified values of the displacement field,

$$\mathbf{e} = \sum_{i=1}^{4} \mathbf{\Phi}_i \mathbf{d}_i, \tag{40}$$

where $\mathbf{d}_i = [\mathbf{u}_i^T,\ \mathbf{v}_i^T,\ \mathbf{w}_i^T]^T$ (as noted before, $\mathbf{w}_2$ and $\mathbf{w}_3$ are $\partial \mathbf{w}_1/\partial t$ and $\partial \mathbf{w}_4/\partial t$, respectively in a TST element) and

$$\mathbf{\Phi}_i = \begin{bmatrix} P_i \mathbf{B}'_{m_u} & 0 & \dfrac{1}{R_s} P_{i\mathrm{H}} \mathbf{B}_{m_w} \\ 0 & P'_i \mathbf{B}_{m_v} & \dfrac{1}{R_s} P_{i\mathrm{H}} \mathbf{B}_{m_w} \\ P'_i \mathbf{B}_{m_u} & P_i \mathbf{B}'_{m_v} & 0 \\ \dfrac{1}{R_s} P_i \mathbf{B}'_{m_u} & 0 & -P_{i\mathrm{H}} \mathbf{B}''_{m_w} \\ 0 & \dfrac{1}{R_t} P'_i \mathbf{B}_{m_v} & -P''_{i\mathrm{H}} \mathbf{B}_{m_w} \\ \dfrac{1}{2}\left(\dfrac{3}{R_s} - \dfrac{1}{R_t}\right) P'_i \mathbf{B}_{m_u} & \dfrac{1}{2}\left(\dfrac{3}{R_t} - \dfrac{1}{R_s}\right) P_i \mathbf{B}'_{m_v} & -2P'_{i\mathrm{H}} \mathbf{B}'_{m_w} \end{bmatrix}. \tag{41}$$

4.2. Stiffness matrix

The stiffness matrix has the same expression as Eq. (29) only in which the definitions of $\mathbf{\Phi}_i$ and $\mathbf{L}$ have changed to Eqs. (41) and (38).

4.3. Geometric stiffness matrix

The matrix $\mathbf{k}_g$ in the geometric stiffness matrix $T\mathbf{k}_g$ has the same expression as Eq. (36). But the definitions for $\mathbf{\Psi}_i$ and $\mathbf{S}$ now change to what follows,

$$\mathbf{\Psi}_i = \begin{bmatrix} P_i \mathbf{B}'_{m_u} & 0 & \dfrac{1}{R_s} P_{i\mathrm{H}} \mathbf{B}_{m_w} \\ P_i \mathbf{B}'_{m_u} & 0 & 0 \\ 0 & P_i \mathbf{B}'_{m_v} & 0 \\ 0 & P'_i \mathbf{B}_{m_v} & \dfrac{1}{R_t} P_{i\mathrm{H}} \mathbf{B}_{m_w} \\ -\dfrac{1}{R_s} P_i \mathbf{B}_{m_u} & 0 & P_{i\mathrm{H}} \mathbf{B}'_{m_w} \\ 0 & -\dfrac{1}{R_t} P_i \mathbf{B}_{m_v} & P'_{i\mathrm{H}} \mathbf{B}_{m_w} \end{bmatrix} \tag{42}$$

and

$$\mathbf{S} = \frac{1}{2\pi y^2(s)} \begin{bmatrix} 0 & 1 & & & & \\ 1 & 0 & & & & \\ & & 0 & 1 & & \\ & & 1 & 0 & & \\ & & & & 0 & 1 \\ & & & & 1 & 0 \end{bmatrix}. \tag{43}$$

5. Solution procedure

Torsional buckling analysis of shells of revolution can finally be expressed as an eigenvalue problem as follows,

$$\mathbf{A}(T)\mathbf{D} = \mathbf{0}, \tag{44}$$

where $\mathbf{A}(T) = \mathbf{K} - T\mathbf{K}_g$, in which $\mathbf{K}$ and $T\mathbf{K}_g$ are the stiffness and geometric stiffness matrices of the shells of revolution, which can be assembled in the standard, direct fashion with those of its elements. Eq. (44) constitutes standard linear eigenvalue problems which could be solved using any of a wide variety methods. To effectively use the axi-symmetric property of the shells of revolution to enhance the efficiency in eigenvalue finding, the Sturm sequence method suggested by Wittrick and Williams (1971) and Gupta (1972) incorporated with a multi-level substructuring technique is used in the present approach. This method evaluates the singularity of the characteristic matrix $\mathbf{A}(T)$ with the variation of T to find its eigenvalue. The lowest T which makes $\mathbf{A}(T)$ singular is the required buckling load for the problem.

When Gauss elimination is used to reduce matrix $\mathbf{A}(T)$ into its triangular form $\mathbf{A}^{\Delta}(T)$, the singularity of $\mathbf{A}(T)$ is equivalent to that one of the elements in the leading diagonal of $\mathbf{A}^{\Delta}(T)$ is zero. That means the singularity happens when $\mathbf{A}(T)$ changes from positive definite to negative definite with the increase of T. Therefore, if T_L and T_U make $\mathbf{A}(T_L)$ and $\mathbf{A}(T_U)$ be positive and negative definite, respectively, the required buckling load T must lie between T_L and T_U. So, bi-section method can be used to find it with certainty.

Based on the fact that any negative definite matrix $\mathbf{A}_s(T)$ which corresponds to a substructure at certain level will cause the negativeness of $\mathbf{A}(T)$ which corresponds to the entire structure, the efficiency to evaluate the positive (or negative) definite property of $\mathbf{A}(T)$ can be dramatically increased using the substructuring technique. This is especially beneficial for the type of structure like the shells of revolution which have axi-symmetric property that can result identical substructures at all levels. In this sense, only the Gauss elimination for those identical substructures at different levels need to be carried out. In the present approach the first level of substructuring involves treating the basic element as a substructure and eliminating freedoms at the internal reference meridians of such an element. The rest of substructuring levels involves sequentially doubling a identical basic element or substructure by taking advantage of the axi-symmetric property of the shells of revolution so that at the end to form a complete shell of revolution. Therefore, the size of the problem is always kept as small as that of a single element in real computation.

The detailed solution procedures are as follows:

Step 1. Divide a shell of revolution into 2^n slender elements circumferentially;

Step 2. Select the initial values of the lower and upper bounds of the buckling load $T_L^{(0)}$ and $T_U^{(0)}$ as 0 and a large number which makes $\mathbf{A}(T_U^{(0)})$ be negative definite, respectively;

Step 3. Use bi-section method to select a new value for T as,

$$T = \frac{\left(T_L^{(k)} + T_U^{(k)}\right)}{2}, (k = 0, 1, 2, \ldots); \tag{45}$$

Step 4. Denote $\mathbf{A}_e(T) = \mathbf{k} - T\mathbf{k}_g$. Now partition $\mathbf{A}_e(T)$ into the form,

$$\mathbf{A}_e(T) = \begin{bmatrix} \mathbf{A}_e(T)^{(\mathrm{II})} & \mathbf{A}_e(T)^{(\mathrm{IO})} \\ \mathbf{A}_e(T)^{(\mathrm{OI})} & \mathbf{A}_e(T)^{(\mathrm{OO})} \end{bmatrix}, \tag{46}$$

in which $\mathbf{A}_e(T)^{(\mathrm{II})}$ and $\mathbf{A}_e(T)^{(\mathrm{OO})}$ are associated with the internal and external degrees of freedom on the internal and external reference meridians of a basic element. Eliminating the internal degrees of freedom obtains the characteristic matrix of the element which is solely associated with the external degrees of freedom of the element. Its expression is as follows:

$$\mathbf{A}_e(T)^{(\mathrm{O})} = \mathbf{A}_e(T)^{(\mathrm{OO})} - \mathbf{A}_e(T)^{(\mathrm{OI})}\left[\mathbf{A}_e(T)^{(\mathrm{II})}\right]^{-1}\mathbf{A}_e(T)^{(\mathrm{IO})}. \tag{47}$$

The local boundary conditions on the internal reference meridians should be taken into account in the above eliminating process. If any element in the leading diagonal of $\mathbf{A}_e^4(T)^{(\mathrm{II})}$ is found to be negative when Gauss elimination is applied on $\mathbf{A}_e(T)^{(\mathrm{II})}$, it can be concluded that matrix $\mathbf{A}_e(T)^{(\mathrm{II})}$ is negative definite so does $\mathbf{A}(T)$ and then go to *Step 6*;

Step 5. Assemble a substructure with two identical elements. Then use the procedure explained in *Step 4* to eliminate the internal degree of freedoms of this substructure, and a characteristic matrix which is only associated with external degree of freedoms of this substructure can be obtained. If the characteristic matrix of this substructure is found to be negative definite during its Gauss elimination process, it can be concluded that this will result $\mathbf{A}(T)$ to be negative definite and then go to *Step 6*. Assemble a higher level substructure with two identical newly obtained substructures and eliminate its internal degree of freedoms. Repeat this doubling process for n times and in the end to form a complete shell of revolution;

Step 6. If $\mathbf{A}(T)$ is negative definite, the new upper bound for the buckling load is modified as $T_U = T$. Otherwise if $\mathbf{A}(T)$ is positive definite, the new lower bound for the buckling load is modified as $T_L = T$;

Step 7. If the relative difference between the two bounds is less than a given precision, then stop the iterative calculation and output the buckling load. Otherwise go back to *Step 3* to start another iteration.

It should be noted that the efficiency of the above solution procedure is not affected by the initial value chosen for $T_{\mathrm{U}}^{(0)}$ because for a large T the negativeness of $\mathbf{A}(T)$ can be detected in its lower substructuring levels which does not involve too much computation at that stage. In finding the buckling load, the majority of the computation is associated with the Gauss elimination. As stated before, the size of the matrix needed to do the Gauss elimination at each level of substructuring is always kept as small as that of the characteristic matrices of a single element and for a shell of revolution with 2^n-element division there are only $n + 1$ such type of Gauss elimination, so the efficiency of Sturm sequence method used in this fashion is very high. This is all due to the axi-symmetric property of the shells of revolution. Once a required buckling load is determined it may be desired to find the corresponding buckling mode shape. The random vector method suggested by Hopper and Williams (1972) is used in the present approach to calculate the buckling mode shape.

6. Applications

The proposed method in the context of SDST and TST has been programmed. Selected torsional buckling applications involving the use of this integrated software are described in what follows. In all applications, the basic elements run the full length of a shell of revolution and four reference meridians are used (i.e. $i_p=4$) in every basic element, and the degree of spline functions for interpolating u, v, w and ψ_t is 3 (i.e. $m_u=m_v=m_w=m_{\psi_t}=3$) and that for ψ_s is 2 (i.e. $m_{\psi_s}=2$).

First, the torsional buckling of an isotropic and an orthotropic circular cylinder with diaphragm ends are analyzed. For the isotropic cylinder the material properties are Young's modulus $E = 100$ GPa, Poisson ratio $\nu=0.3$ and for the orthotropic cylinder the material properties are Young's modulus $E_L=100$ GPa, $E_T=20$ GPa, Poisson ratio $\nu=0.3$ and shear modulus $G_{LT}=G_{TT}=8.5$ GPa. The length (L) and radius (R) of the cylinder are 0.5 m and 0.1 m. Ten equal spline sections and 256 elements arranged in nine levels of substructures are used in the proposed method. The calculated buckling loads (T) using TST analysis are recorded in Table 1. For comparison, the prediction for these loads obtained using the following approximate formula,

$$T_{\mathrm{cr}} = 21.75D_{22}^{5/8}\left(\frac{A_{11}A_{22}-A_{12}^2}{A_{22}}\right)^{3/8}\frac{R^{5/4}}{L^{1/2}}, \tag{48}$$

which was given by Vinson and Sierakowski (1986) are also recorded in Table 1. The validity of the above approximate solution depends on the following condition (see, e.g. Vinson and Sierakowski, 1986),

$$r = 500\left(\frac{D_{11}}{D_{22}}\right)^{5/6}\left(\frac{12A_{22}D_{11}}{A_{11}A_{22}-A_{12}^2}\right)^{1/2}\frac{R}{L^2}\leq 1. \tag{49}$$

This quantity is also calculated and recorded in Table 1. The relative difference e between the two results is calculated as $e=(T_{\mathrm{cr}}-T)/T_{\mathrm{cr}}$ and is given in Table 1 too. It can be seen from Table 1 that when r is very small, the two results come closer.

Next, the torsional buckling behaviours of a circular shell, a conic shell, an elliptic hyperboloid shell and an ellipsoid shell, each of them having isotropic material properties, cross-ply and angle-ply laminations, are analyzed using both TST and SDST theory. In the present case, all shells are clamped at one end and simply supported at another. Their lengths are all 0.5 m and their thicknesses all change from 0.0005 m to 0.001 m and to 0.002 m to model the thin and thick shells. The radius of all shells at the clamped end are same with value of 0.1 m. The radius of the conic, the elliptic hyperboloid and the ellipsoid shells at the simply supported end are the same, with avalue of 0.07 m. The radius of the

Table 1
Comparison of the buckling loads (Nm) obtained by the proposed method and the approximate analytical method. (The values in parentheses are calculated with Eq. (48))

Thickness h (cm)	Isotropic material			Orthotropic material		
	T	e	r	T	e	r
0.05	1374.1 (1431.7)	4.02%	10.7%	423.35 (502.83)	15.8%	38.9%
0.02	175.65 (182.17)	3.58%	4.27%	56.201 (63.984)	12.2%	15.6%
0.01	37.141 (38.297)	3.02%	2.14%	12.118 (13.454)	9.91%	7.78%
0.001	0.2092 (0.2154)	2.86%	0.21%	0.0713 (0.0756)	5.67%	0.78%

elliptic hyperboloid and the ellipsoid shells at 0.3 m away from the clamped end are 0.05 m and 0.12 m, respectively. The meridians of the elliptic hyperboloid and the ellipsoid shells are parabola. For the isotropic shells, the material properties are the same as those used in the first example. For the laminated composite shells, two layers of equal thickness are used which have the same orthotropic material properties as described in the first example. In the shells with cross-ply laminations the lay-up is $[0^\circ/90^\circ]$, i.e. the inner layer is placed along the meridian whilst the outer layer is placed 90° to the meridian. In the shells with angle-ply laminations the lay-up is $[45^\circ/90^\circ]$, i.e. the inner layer is placed 45° to the meridian and the outer layer remains the same as in the cross-ply shells. As an overall buckling mode shape happens for the circular, the conic and the elliptic hyperboloid shells, ten spline sections evenly distributed along the meridian and 256 elements arranged in nine levels of substructures as in the first example are used. However, as a local buckling mode shape happens for the ellipsoid shell, ten unequal spline sections with knot sequence [0, 0.13, 0.25, 0.35, 0.385, 0.415, 0.44, 0.46, 0.475, 0.49, 0.50909] m are used in this case, and the number of elements used is the same as before. For comparison, twenty equal spline sections are also used to try to capture the local buckling mode shapes. The calculated buckling loads are recorded in Table 2 and some of the buckling mode shapes are shown in Figs. 3–10.

It can be seen from Table 2 that when the shells are thin the buckling loads obtained from TST and SDST models are very close as expected and when the shells become gradually thicker the buckling loads obtained from these two models deviate from each other to an extent which can be as big as over one percent in the case of thick ($h = 0.002$ m) elliptic hyperboloid angle-ply shells for which the shell thickness to its minimum circumferential radius ratio is one over twenty five. From Figs. 3–10, it can be seen that with the increase of the shell thickness the number of circumferential half waves of the buckling mode shapes reduces. This is because the contribution from the bending deformation to the shell strain energy increases with the increase of the shell thickness. In comparing the results obtained using twenty equal and ten unequal spline sections for the ellipsoid shells, it is found that in most cases the buckling loads obtained corresponding to twenty equal spline sections are higher than what are

Table 2
Buckling loads (Nm) of different shells of revolution. (The values in parentheses are obtained using twenty equal spline sections)

Thickness	Material property	Theory	Circular shell	Conic shell	Elliptic hyperboloid shell	Ellipsoid shell
0.0005 m	Isotropic material	TST	1448.0	1136.6	436.46	2963.4 (2992.0)
		SDST	1447.1	1135.9	436.90	2961.1 (3008.7)
	Cross-ply laminates	TST	530.95	421.07	163.93	934.75 (964.58)
		SDST	530.57	420.78	163.68	933.23 (966.49)
	Angle-ply laminates	TST	486.18	379.63	171.15	1025.6 (1025.7)
		SDST	485.72	379.26	170.64	1023.7 (1024.6)
0.001m	Isotropic material	TST	6871.1	5377.3	2291.9	12979.0 (13029.0)
		SDST	6861.9	5369.5	2290.5	12936.0 (12983.0)
	Cross-ply laminates	TST	2430.3	1915.1	826.01	4023.1 (4091.8)
		SDST	2426.0	1911.6	818.69	3997.6 (4058.1)
	Angle-ply laminates	TST	2361.6	1837.5	842.82	4567.5 (4552.9)
		SDST	2356.8	1833.7	839.41	4539.4 (4530.0)
0.002m	Isotropic material	TST	32816.0	25233.0	11227.	57271.0 (57315.0)
		SDST	32723.0	25146.0	11179.	56768.0 (56859.0)
	Cross-ply laminates	TST	11047.0	8630.7	3834.6	17586.0 (17656.0)
		SDST	10997.0	8593.0	3801.5	17395.0 (17468.0)
	Angle-ply laminates	TST	11396.0	9271.5	4654.7	20389.0 (20264.0)
		SDST	11341.0	9231.7	4592.9	20107.0 (20085.0)

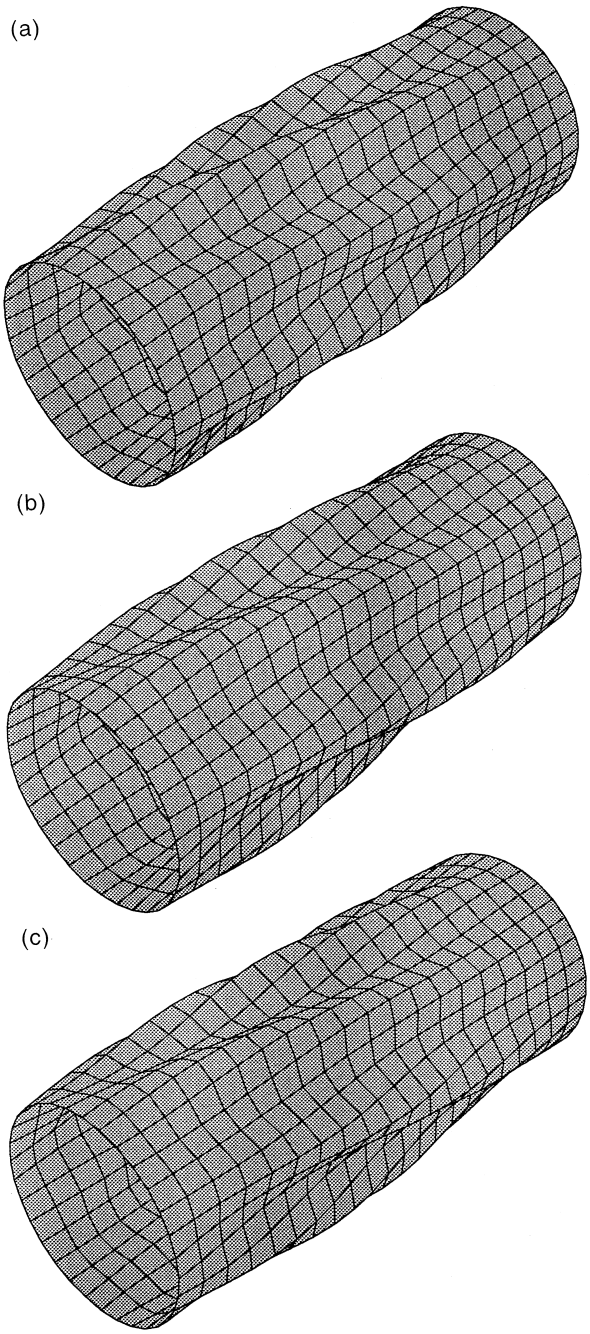

Fig. 3. Torsional buckling mode shapes of a thin circular shell. (Isotropic (a), Cross-ply (b) and Angle-ply (c); $h = 0.0005$ m).

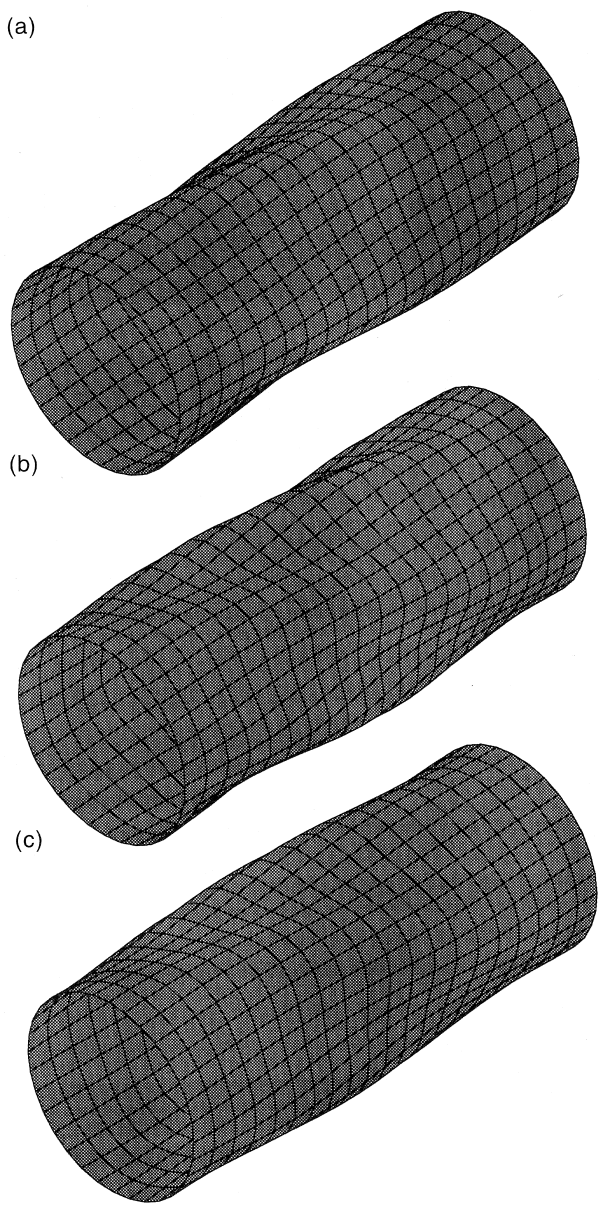

Fig. 4. Torsional buckling mode shapes of a thick circular shell. (Isotropic (a), Cross-ply (b) and Angle-ply (c); $h = 0.002$ m).

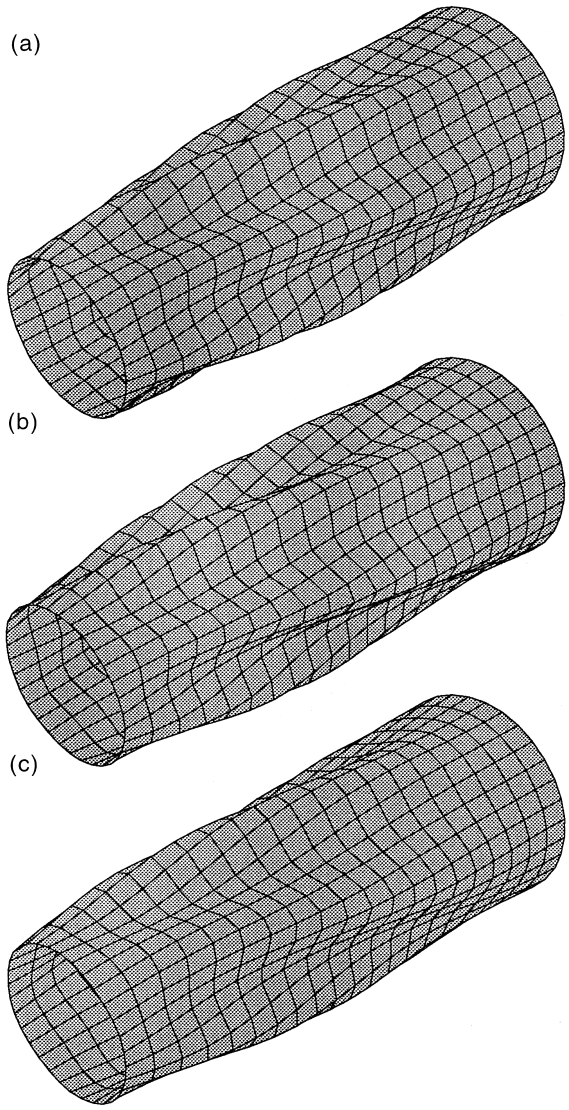

Fig. 5. Torsional buckling mode shapes of a thin conic shell. (Isotropic (a), Cross-ply (b) and Angle-ply (c); $h = 0.0005$ m).

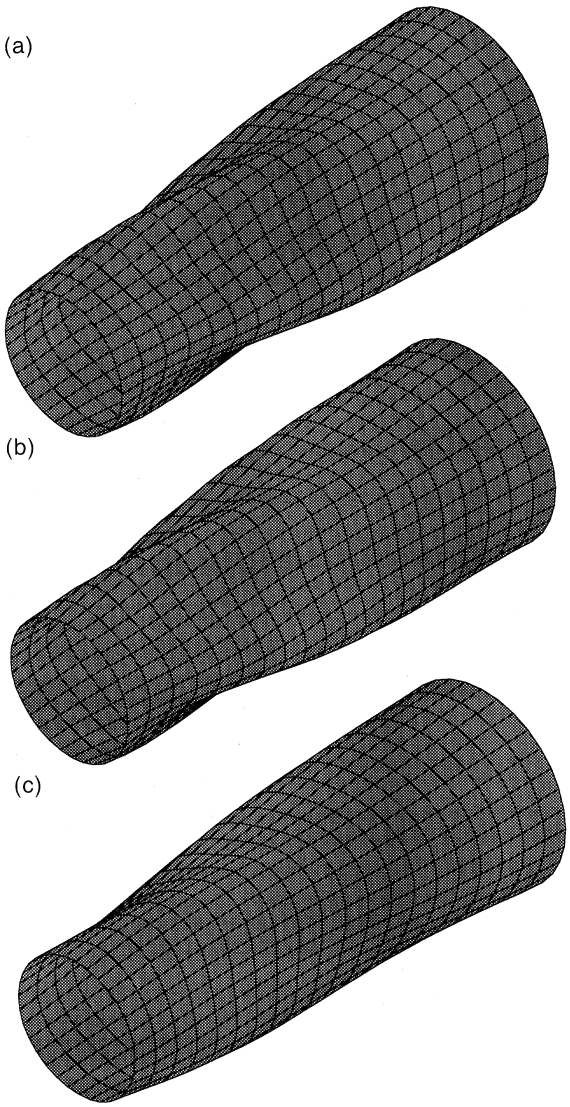

Fig. 6. Torsional buckling mode shapes of a thick conic shell. (Isotropic (a), Cross-ply (b) and Angle-ply (c); $h = 0.002$ m).

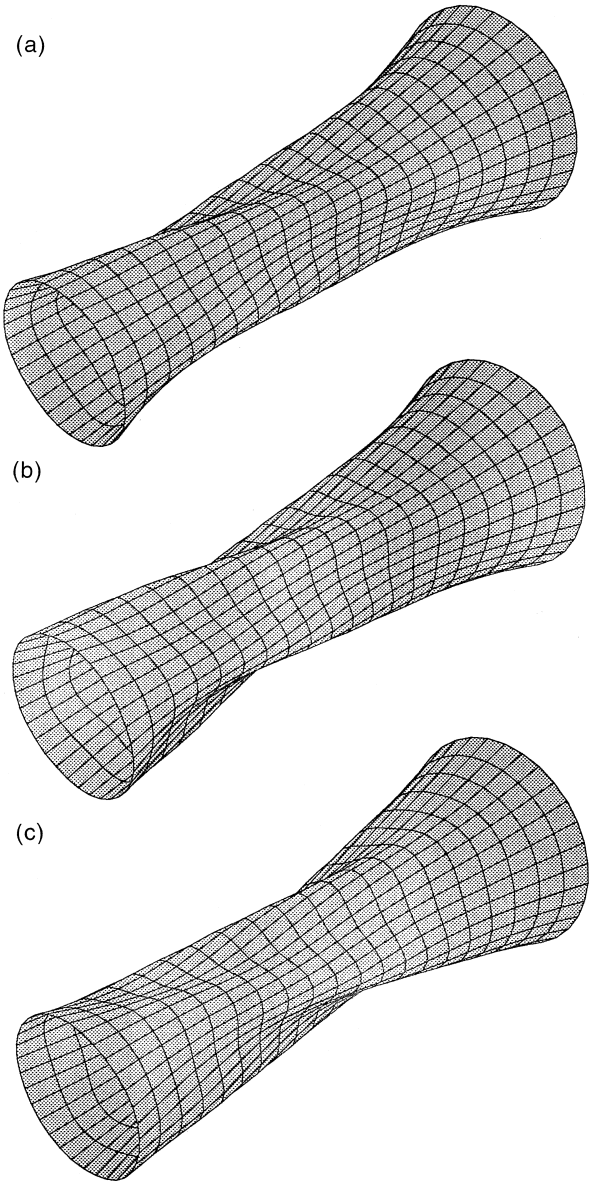

Fig. 7. Torsional buckling mode shapes of a thin elliptic hyperboloid shell. (Isotropic (a), Cross-ply (b) and Angle-ply (c); h = 0.0005 m).

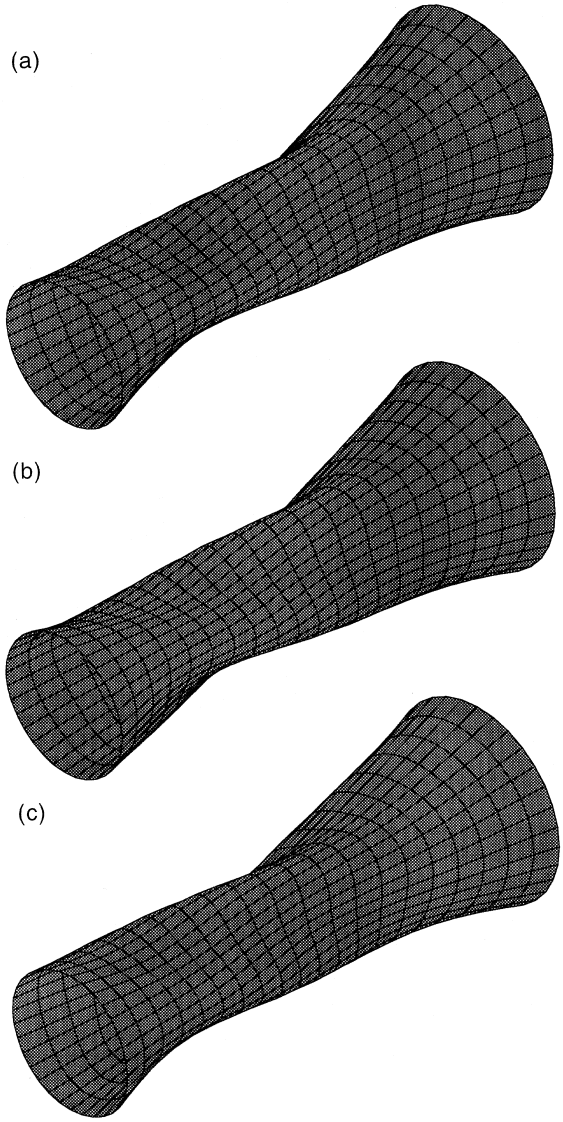

Fig. 8. Torsional buckling mode shapes of a thick elliptic hyperboloid shell. (Isotropic (a), Cross-ply (b) and Angle-ply (c); h = 0.002 m).

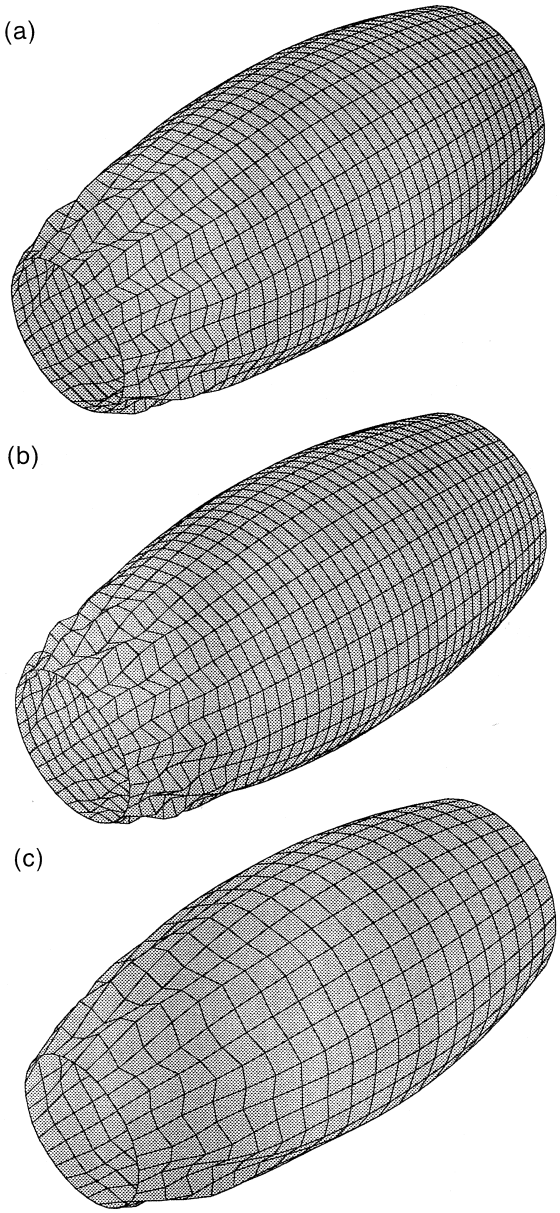

Fig. 9. Torsional buckling mode shapes of a thin ellipsoid shell. (Isotropic (a), Cross-ply (b) and Angle-ply (c); $h = 0.0005$ m).

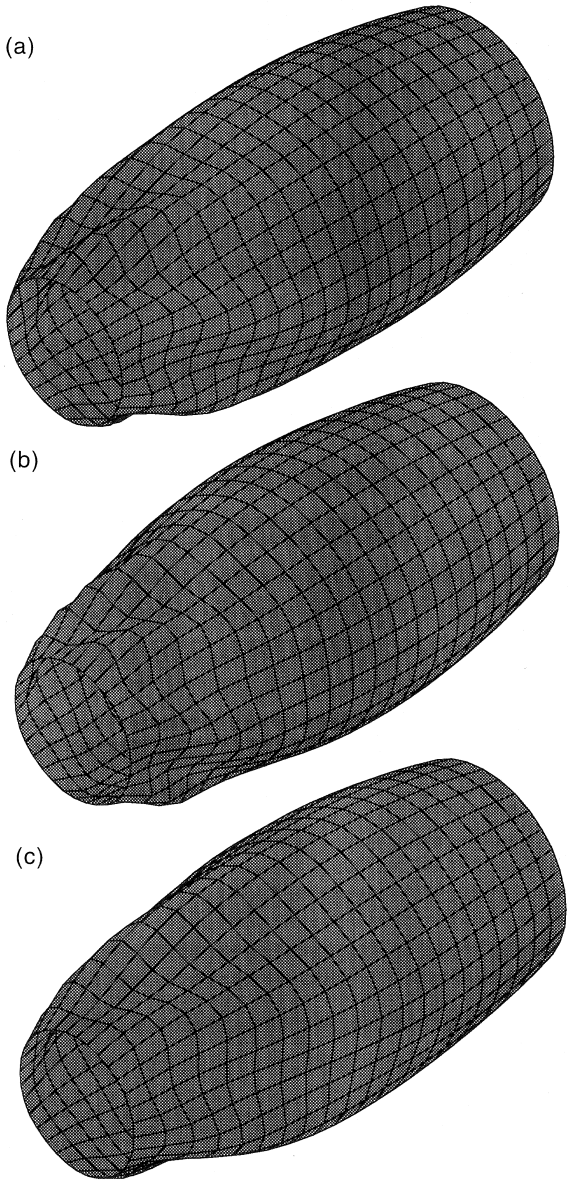

Fig. 10. Torsional buckling mode shapes of a thick ellipsoid shell. (Isotropic (a), Cross-ply (b) and Angle-ply (c); $h = 0.002$ m).

obtained using ten unequal spline sections although the degree of freedoms in the former is much larger than that in the latter. Only in the cases of thicker ($h = 0.001$ m and 0.002 m) angle-ply ellipsoid shells whose buckling mode shapes are not very localized as seen from Fig. 10(c), the buckling loads obtained using twenty equal spline sections are slightly better than that obtained using ten unequal spline sections. This particular example also shows the advantages of the general spline method for local buckling problems.

7. Conclusions

Two types of shell elements based on the displacement descriptions in the thin shell theory and the first-order shear deformation shell theory have been developed using Rayleigh–Ritz approach. They are featured with good displacement continuity along the meridians of the shells of revolution because of the spline functions used in the displacement interpolation in that direction. Under the static equilibrium condition and small pre-buckling displacement assumption, the pre-buckling shear stress distribution is determined and the torsional buckling problem is formed for the shells of revolution using the stiffness and geometric stiffness matrices constructed with respect to their original geometries. Numerical examples have been successfully carried out to show the validity of these two models and particularly their capability to capture the local buckling mode shapes with less computational efforts.

Acknowledgements

The author would like to thank the referees for their helpful comments.

References

Crisfield, M.A., Peng, X., Shi, J., 1992. Some recent developments with shell and stability analysis. In: Ladeveze, P., et al. (Eds.), New Advances in Computational Structural Mechanics. Elsevier Science, pp. 249–258.

Gupta, K.K., 1972. Solution of eigenvalue problems by Sturm sequence method. International Journal of Numerical Methods in Engineering 4, 379–404.

Hopper, C.T., Williams, F.W., 1972. Mode finding in nonlinear structural eigenvalue calculations. J. Struct. Mech. 5, 255–278.

Leissa, A.W., Chang, J.-D., 1996. Elastic deformation of thick, laminated composite shells. Composite Structures 35, 153–170.

Reddy, J.N., 1984. Exact solution of moderately thick laminated shells. J. Engng. Mech. Div., ASCE 110, 794–805.

Schempp, W., 1982. Complex Contour Integral Representation of Cardinal Spline Functions. American Mathematical Society.

Stolarski, H., Belytschko, T., Lee, S.-H., 1995. Review of shell finite element and corotational theories. Computational Mechanics Advances 2, 125–212.

Vinson, J.R., Sierakowski, R.L., 1986. The Behaviour of Structures Composed of Composite Materials. Nijhoft, Dordrecht.

Wittrick, W.H., Williams, F.W., 1971. A general algorithm for computing natural frequencies of elastic structures. Q. J. Mech. and Appl. Math. 24, 263–284.